Synthesis of coral-globular-like composite Ag/TiO_2-SnO_2 and its photocatalytic degradation of rhodamine B under multiple modes

Q. Song, L. Li, N. Zhuo, H. N. Zhang, X. Chen and Y. X. Li

ABSTRACT

Taking cetyltrimethylammonium bromide (CTAB) as the template and using TiO_2 as the substrate, coral-globular-like composite Ag/TiO_2-SnO_2 (CTAB) was successfully synthesized by the sol–gel combined with a temperature-programmed treatment method. X-ray diffraction, scanning electron microscopy (SEM), UV–vis diffuse reflectance spectroscopy, X-ray photoelectron spectroscopy, SEM combined with X-ray energy dispersive spectroscopy, and N_2 adsorption–desorption tests were employed to characterize samples' crystalline phase, chemical composition, morphology and surface physicochemical properties. Results showed that composites not only had TiO_2 anatase structure, but also had some generated $SnTiO_4$, and the silver species was metallic Ag^0. Ag/TiO_2-SnO_2 (CTAB) possessed a coral-globular-like structure with nanosheets in large quantities. The photocatalytic activity of Ag/TiO_2-SnO_2 (CTAB) had studied by degrading organic dyes under multi-modes, mainly using rhodamine B as the model molecule. Results showed that the coral-globular-like Ag/TiO_2-SnO_2 (CTAB) was higher photocatalytic activity than that of commercial TiO_2, Ag/TiO_2-SnO_2, TiO_2-SnO_2 (CTAB), and TiO_2-SnO_2 under ultraviolet light irradiation. Moreover, Ag/TiO_2-SnO_2 (CTAB) composite can significantly affect the photocatalytic degradation under multi-modes including UV light, visible light, simulated solar light and microwave-assisted irradiation. Meanwhile, the photocatalytic activity of Ag/TiO_2-SnO_2 (CTAB) was maintained even after three cycles, indicating that the catalyst had good usability.

Key words | Ag/TiO_2-SnO_2, cetyltrimethyl ammonium bromide, multi-mode photocatalysis, rhodamine B, sol-gel, temperature-programmed hydrothermal treatment

Q. Song
L. Li (corresponding author)
H. N. Zhang
College of Materials Science and Engineering,
Qiqihar University,
Qiqihar 161006,
China
E-mail: *qqhrll@163.com*; *qqhrlili@126.com*

Q. Song
L. Li
N. Zhuo
X. Chen
Y. X. Li
College of Chemistry and Chemical Engineering,
Qiqihar University,
Qiqihar 161006,
China

L. Li
College of Heilongjiang Province Key Laboratory of Fine Chemicals,
Qiqihar 161006,
China

INTRODUCTION

In recent years, with environmental pollution increasing, photocatalysis as a kind of advanced technology has shown huge potential for pollutant degradation, energy conversion, selective oxidation, and organic synthesis. In all kinds of methods of water pollution treatment, the semiconductor photocatalysis technology has been widely studied due to its environment-friendliness, and lower cost (Liao *et al.* 2008; Chen *et al.* 2013). The photocatalytic technology usually refers to the photocatalytic reaction occurring light irradiation if the light energy is the same as or higher than the band gap of the semiconductor. That is, the semiconductor absorbs the light energy and is excited, resulting in photogenerated electrons gathering on the conduction band and photogenerated holes on the valence band. Photogenerated electrons and photogenerated holes react with molecules (oxygen adsorption, surface hydroxyl group or water) absorbed on the surface of the semiconductor, respectively, generating strong oxidizing substances such as the superoxide radical ($\cdot O_2^-$) and the hydroxyl free radical ($\cdot$OH) that can react with organic pollution molecules, so that organic molecules are degraded and mineralized by active groups (Fan *et al.* 2009; Yuan *et al.* 2011; Dimitrijevic *et al.* 2013). However, according to relatively recent research, band gaps of some pure semiconductor materials are wide and the semiconductors have low efficiencies for light (Liang *et al.* 2012; Li *et al.* 2014a), of which the practical application is limited to some extent. Researchers have carried out a lot of work, including increasing the light

doi: 10.2166/wst.2017.323

response range, promoting the transfer of the interface charge, and decreasing the recombination of photogenerated electrons and photogenerated holes to improve the photocatalytic activity of TiO_2, SnO_2, and other semiconductor materials. Examples include the following.

(a) Noble metal doped. Fermi levels of Ag, Au, Pt, Pd, etc. are lower, with noble metal depositing on the surface of the semiconductor, and the Schottky barrier can be formed to capture photogenerated electrons, thus effectively reducing the recombination of electrons and holes (Chen *et al.* 2014; Li *et al.* 2014b).
(b) Semiconductor composited. Semiconductors (WO_3, SnO_2, ZnO, etc.) are compounded with different band width gap to improve the utilization rate of the solar spectrum (Li *et al.* 2014c).
(c) The template used. The template is conducive to the formation of a special surface, thus changing the specific surface area and the pore size of the semiconductor material, which further improves the photocatalytic activity owing to charge carriers being effectively transferred (Merrill *et al.* 2013; Jiang *et al.* 2015).

On the basis of research, we take cetyltrimethyl ammonium bromide (CTAB) as the template and use TiO_2 as the substrate to synthesize Ag/TiO_2-SnO_2 (CTAB) by the sol–gel combined with temperature-programmed treatment method in this paper. The main ideas of the synthesized design are as follows. (1) TiO_2 (3.2 eV) and SnO_2 (3.8 eV) are relatively common semiconductor photocatalytic materials, whose band gaps are different; through the coupling of TiO_2 and SnO_2, using the synergistic effect to increase the light response range, the photocatalytic activity is improved (Beltran *et al.* 2008; Katoch *et al.* 2015). (2) During the synthesis process, noble metal Ag is doped to take advantage of the electron capture ability of Ag to decrease the recombination of photogenerated electrons and photogenerated holes. At the same time, surface plasmon resonance (SPR)) effect of Ag makes the composite absorption in the visible region, thus enhancing the photocatalytic activity (Li *et al.* 2008; Shan *et al.* 2013). (3) In the synthesis reaction, the template CTAB is added. Utilizing the electrostatic and steric effect of CTAB to influence the growth direction of the composite in the process of synthesis, a better morphology of the composite is obtained (Pan *et al.* 2011; Kumar *et al.* 2014).

Under the above guidance ideas, we expect that Ag/SnO_2-TiO_2 (CTAB) composite can form a special structure and has an excellent morphology under the action of the template CTAB and Ag. In addition, we select rhodamine B (RhB) as the model molecule to study the photocatalytic activity of the as-synthesized Ag/SnO_2-TiO_2 (CTAB) under multi-mode photocatalysis.

EXPERIMENTAL

Materials

Tetra isopropyl titanate (TTIP, 98%) was purchased from Shenzhen Chunhe Merrill Chemical Technology Limited Company. Methanol (CH_3OH, 99.5%) and isopropanol ($CH_3CHOHCH_3$, 99.7%) were purchased from Tianjin Tianli Chemical Reagent Factory. Tert-butanol was purchased from Meryer (Shanghai) Chemical Technology Co., Ltd. Ethylenediamine tetraacetic acid disodium salt, silver nitrate ($AgNO_3$) and CTAB were purchased from Tianjin Kaitong Chemical Reagent Limited Company. Crystalline stannic chloride ($SnCl_4{\cdot}5H_2O$, 99%) was purchased from Tianjin Guangfu Institute of Fine Chemicals. RhB, methylene blue (MB), methyl orange (MO), salicylic acid (SA) and neutral red (NR) were purchased from Beijing chemical plant. All reagents are analysis pure. Deionized and doubly distilled water was used in all the experiments.

Synthesis of Ag/SnO_2-TiO_2 (CTAB)

In the typical process, according to the molar ratio of Ag:Ti:CTAB = 0.1:1:0.05, $AgNO_3$, TTIP, and CTAB were added to 10 mL isopropanol solution under stirring at room temperature to form a water gel. Then the water gel was transferred into a Teflon-lined autoclave and heated at 160 °C (2 °C/min) for 24 h and cooled down to the room temperature naturally. $SnCl_4$ solution (0.75 mmol) was added to the above Teflon-lined autoclave under stirring, ultrasonicated for 30 min, kept at 160 °C (2 °C/min) for 24 h then cooled down to room temperature. The as-prepared product (molar ratio of Ti:Sn = 13.33:1) was washed three times with the deionized water and ethanol, dried at 80 °C for 10 h, and finally calcined at 600 °C for 7 h. Ag/TiO_2-SnO_2, TiO_2-SnO_2 (CTAB), and TiO_2-SnO_2 were synthesized by the same method without adding CTAB or silver nitrate solution in the process.

Characterization

X-ray diffraction (XRD) pattern was used to analyze the crystalline structure by the XRD analysis (German Bruker-AXS (D8) with Cu Kα as X-ray radiation under 60 kV and 80 mA and with the 2θ ranging from 20° to 80°). Scanning electron microscopy (SEM) with energy dispersive spectroscopy (EDS) was undertaken using an S-4300 SEM, Hitachi,

working voltage 5 kV. The X-ray photoelectron spectroscopy (XPS) spectra of the samples were measured with a VG-ADES400X, using a MgK-ADES source; the residual gas pressure was less than 10^{-8} Pa. UV–vis diffuse reflectance spectra (UV–vis/DRS) were recorded with a UV–vis spectrophotometer (TU-1901, Beijing General Analytical General Company, China) using $BaSO_4$ as reflectance standard. The absorbance of sample solution was determined by the TU-1901 UV–vis double-beam spectrophotometer. The surface area and pore size of sample were obtained using Quanchrome NoveWin2 USA Contador physisorption apparatus, with a measuring temperature of 77 K.

Multiple mode photocatalytic degradation tests

The photocatalytic activities of the as-synthesized composite material Ag/TiO_2-SnO_2 (CTAB) were evaluated by photocatalytic degradation of RhB under multi-modes including UV, visible light, microwave-assisted and simulated solar light. The experimental device is composed of a cylindrical quartz outer tube and a quartz glass sleeve in which a built-in visible light source is a 400 W Xe lamp (the main emission line is greater than 410 nm, the inner sleeve is made of No. 11 glass to filter out the ultraviolet light emitted). The ultraviolet light source is a 125 W high-pressure mercury lamp (the wavelength of the main emission line is about 313.2 nm). The microwave-assisted photocatalytic device is made of a quartz tube, filled with metal mercury and inert gas Ar; the emission wavelength is about 280 nm and the power is 15 W. Simulated sunlight photocatalytic reaction is formed by a BL-GHX-V photocatalytic reactor: the light source is a 1,000 W external Xe lamp (external type, Shanghai Bison Instruments Co. Ltd, the emission spectrum was close to the full spectrum), distance 8.5 cm between the lamp and the reaction liquid, constant temperature by ethanol recycling equipment for keeping the temperature in the reaction system. RhB was used as the model dye molecule, but MB, MO, SA and NR were also involved in those photocatalytic experiments under UV light irradiation.

(1) UV light mode: 0.15 g photocatalysts was suspended in 90 mL of RhB solution (50 mL/L) under ultrasonication for 10 min, then stirred for 30 min in the dark to ensure the adsorption/desorption equilibrium between RhB and photocatalyst powders. The high-pressure mercury lamp was placed into a jacketed quartz tube that was soaked in the solution, magnetically stirred continuously, and suspensions were kept at constant temperature by circulating water through the jacket during the entire process. Three millilitres of suspension was sampled and centrifuged to remove the photocatalyst particles. Then, the absorption spectrum of the centrifuged solution was recorded using a TU-1901 UV–vis spectrophotometer. The change in RhB concentration was determined by monitoring the optical intensity of the absorption spectra at 499 nm.
(2) Visible light mode: 0.30 g photocatalyst was suspended in 220 mL of RhB solution (50 mL/L). Other steps of the degradation were the same as the UV mode, except the lamp source was a 400 W Xe lamp.
(3) Microwave-assisted mode: 500 mL of RhB (50 mg/L) solution and 0.50 g photocatalysts were placed in a microwave reactor and stirred for 30 min in the dark to ensure the adsorption/desorption equilibrium between RhB and photocatalyst powders. The microwave reactor employed for the degradation of RhB was purchased from Yuhua Instrument Limited Company of China. It consisted of a cylindrical glass reactor (capacity 600 mL) with a 600 mm long water reflux condenser, connected through a communication pipe. The microwave discharge electrode lamp (MDEL) was placed into the reaction solution, with about two-thirds of the MDEL being in the reaction solution. Three silicone tubes were connected to the equipment, which could let water in and out, and let air out through the hole in the microwave reactor. Air was bubbled into the solution through a sintered glass filter, fixed at the bottom of the reactor for passing oxygen, as well as for mixing the catalyst and the solution. At given time intervals, 3 mL of suspension was sampled and centrifuged to remove the photocatalyst particles. Then, the absorption spectrum of the centrifuged solution was recorded using a TU-1901 UV–vis spectrophotometer.
(4) Simulated solar light mode. D: during the process of the simulated solar light irradiation, 90 mL of RhB (50 mg/L) solution and 0.15 g photocatalysts were placed in a quartz photoreactor and stirred for 30 min in the dark. The subsequent steps of the experiment were the same as for the UV light mode above, except the lamp source was a 1,000 W external Xe lamp.

To determine the photocatalytic oxidation pathways of the as-synthesized composite Ag/TiO_2-SnO_2 (CTAB), tert-butanol (1 mM), ethylenediamine tetraacetic acid disodium salt (1 mM, EDTA), and methanol (1 mM) were selected as scavenger agents for oxygen radical anions, holes and hydroxyl radicals, respectively, for the photocatalytic degradation of RhB over Ag/TiO_2-SnO_2 (CTAB) under UV light irradiation. Other steps of the degradation were the same as the UV mode.

RESULTS AND DISCUSSION

XRD analysis

The XRD pattern was used to analyze the crystalline structure of Ag/TiO_2-SnO_2 (CTAB) composite, contrasted with these patterns of Ag, TiO_2, and SnO_2. The results are shown in Figure 1(a). Characteristic diffraction peaks of pure Ag are located at 38.21°, 44.47°, 64.47° and 77.48°, corresponding to the cubic phase (03-0921 JCPDS). Pure TiO_2 shows anatase phase, and its characteristic diffraction peaks are located at 25.31°, 37.90°, 48.02°, 54.64° and 62.83° (21-1272 JCPDS). Characteristic diffraction peaks of SnO_2 are located at 26.6°, 33.9°, 37.9°, 51.8° and 54.8° (41-1445 JCPDS), corresponding to the tetragonal rutile phase. From Figure 1(a), not only does the XRD pattern of Ag/TiO_2-SnO_2 (CTAB) composite show characteristic diffraction peaks of not only anatase TiO_2 and tetragonal rutile SnO_2 phase that are existing in the composite, but also a new substance, $SnTiO_4$, is produced whose characteristic diffraction peaks are located at 27.0°, 34.9° and 53.0°, indexed to tetragonal phase of $SnTiO_4$ (70-4407 JCPDS), corresponding to (110), (101) and (211) crystal planes (Mishra *et al.* 2010; Xu *et al.* 2012). However, characteristic diffraction peaks of Ag are weaker in the XRD patterns, due to lower Ag addition in the synthesis process. The diffraction peaks of TiO_2 are weaker due to $SnTiO_4$ generated in the synthesis process (Chen *et al.* 2000), and the diffraction peak of SnO_2 located at $2\theta = 37.9°$ is close to that of Ag located at $2\theta = 38.21°$, leading to the overlap of peaks. It is the reason why characteristic diffraction peaks of Ag are not apparent in the diffraction pattern of the Ag/TiO_2-SnO_2 (CTAB).

At the same time, in order to further investigate the effect of the CTAB template action and Ag deposition on diffraction peaks of as-synthesized composites, four kinds of as-synthesized composites, Ag/TiO_2-SnO_2 (CTAB), TiO_2-SnO_2 (CTAB), Ag/TiO_2-SnO_2, and TiO_2-SnO_2, were analyzed by XRD analysis, shown in Figure 1(b). According to the Scherrer formula, crystallite sizes of as-composites were calculated and are shown in Table 1. From Table 1, the crystallite size of Ag/TiO_2-SnO_2 (CTAB) is significantly increased; in addition, the crystal structure of composites is not obviously changed through the CTAB action.

UV–vis/DRS analysis

The UV–vis diffuse reflectance absorption spectrum was used to investigate the light absorption ability of the four kinds of composites. Band gap energies of pure TiO_2 (3.2 eV) and SnO_2 (3.8 eV) are wide, and mainly absorb light in the ultraviolet region. From Figure 2(a), Ag/TiO_2-SnO_2 (CTAB) and Ag/TiO_2-SnO_2 composites not only have strong absorption in the ultraviolet region but also show a certain optical absorption in the visible region. The absorption intensity of composite materials with Ag deposition is larger than that of those without Ag deposition, indicating that the optical absorption ability of composites is enhanced with Ag deposition, in which the peak is red-shifted to the visible region. Compared with other samples, Ag/TiO_2-SnO_2 (CTAB) exhibits a certain activity in the visible light (Li *et al.* 2011), attributed to the surface plasmon absorption effect of Ag.

According to the Kubelka–Munk energy curves made by above results, band gap energy (Eg) values of Ag/TiO_2-SnO_2 (CTAB), Ag/TiO_2-SnO_2, TiO_2-SnO_2 (CTAB), and TiO_2-SnO_2

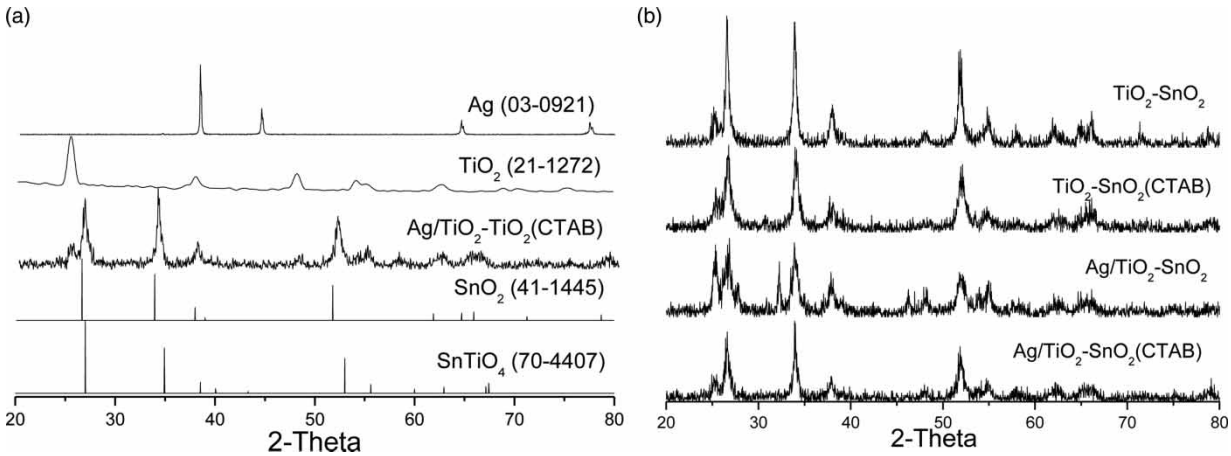

Figure 1 | XRD patterns of Ag, TiO_2, SnO_2, $SnTiO_4$, and as-synthesized Ag/TiO_2-SnO_2 (CTAB) (a); XRD patterns of as-synthesized Ag/TiO_2-SnO_2 (CTAB), Ag/TiO_2-SnO_2, TiO_2-SnO_2, and TiO_2-SnO_2 (CTAB) (b).

Table 1 | The band gap energy (Eg), average pore diameter (D), BET surface area (S_{BET}), crystallite size (D^*) and pore volume (V_{total}) of Ag/TiO_2-SnO_2 (CTAB), Ag/TiO_2-SnO_2, TiO_2-SnO_2, and TiO_2-SnO_2 (CTAB)

Sample	Ag/TiO_2-SnO_2 (CTAB)	Ag/TiO_2-SnO_2	TiO_2-SnO_2 (CTAB)	TiO_2-SnO_2
Eg (eV)	2.63	2.74	3.34	3.40
D (nm)	40.96	13.06	16.67	23.90
S_{BET} (m^2/g)	43.94	36.54	52.03	49.69
D* (nm)	9.18	7.81	7.55	8.45
V_{total} (cm^3/g)	0.122	0.095	0.139	0.134

D* is the average crystallite size of sample calculated using the Scherrer equation.

were calculated and are shown in Table 1, respectively. Seen from Table 1, band gaps of Ag/TiO_2-SnO_2 (CTAB) and Ag/TiO_2-SnO_2 composite materials are lower than that of TiO_2-SnO_2 (CTAB) and TiO_2-SnO_2, indicating that the former two composites will show good photocatalytic capability.

XPS analysis

XPS analysis is used to examine the surface element composition and chemical state of Ag/TiO_2-SnO_2 (CTAB). The XPS survey spectra are shown in Figure 3(a), revealing no peaks of elements other than Ti, O, Ag, Sn, and C in the sample, evidencing purity of the sample. The presence of C is ascribed to adventitious hydrocarbon from the XPS instrument itself (Gao *et al.* 2004). As shown in Figure 3(b), two peaks of the sample can be attributed to $Ag_{3d5/2}$ and $Ag_{3d3/2}$ spectra, corresponding to the binding energy of 367.8 and 373.8 eV, respectively, indicating that Ag in the product exists in the form of Ag^0 (Kobayashi *et al.* 2014; Kumar *et al.* 2014). These results further confirm the above XRD observation; moreover, characteristic peaks of Ag^0 are detected, implying that Ag^0 indeed exists in the product (Wu *et al.* 2010).

SEM analysis

The detailed morphology and the microstructure of sample were inspected by SEM analysis. Figure 4 presents a series of SEM images of Ag/TiO_2-SnO_2 (CTAB) in different scales. From Figure 4(b), we can find that Ag/TiO_2-SnO_2 (CTAB) under the action of template agent CTAB shows a regular coral-globular structure with the radius of about 3 μm. As seen from Figure 4(d), the surface of the sphere shows a dense lamellar structure, and the length of the nanosheet is about 1 μm; at the same time, there are also small particles. The formation of the coral-globular structure is mainly caused by the integrated effect of noble metal Ag and CTAB. On the one hand, Ag as the precious metal element has the optical rotation of size and shape that can influence the internal structure of the product, so that the morphology of the product is changed to a certain extent (Chen *et al.* 2014). On the other hand, CTAB as the cationic surfactant can form cationic $C_{19}H_{42}N^+$ with hydrophobic group that can affect the growth direction of composite material by electrostatic and steric effects. Moreover, an electric double layer can be formed on the surface in the synthesis of particles, which can reduce the surface energy of ions of the as-synthesized sample to some extent, restraining

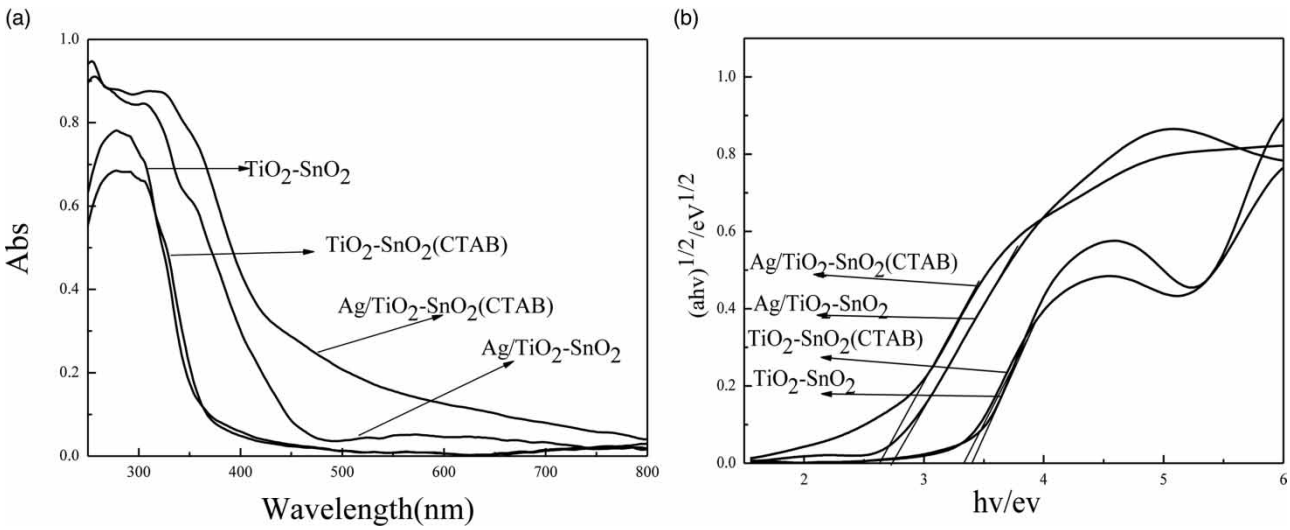

Figure 2 | UV–vis/DRS of the as-synthesized samples (a) and the Kubelka-Munk energy curves of as-synthesized samples (b).

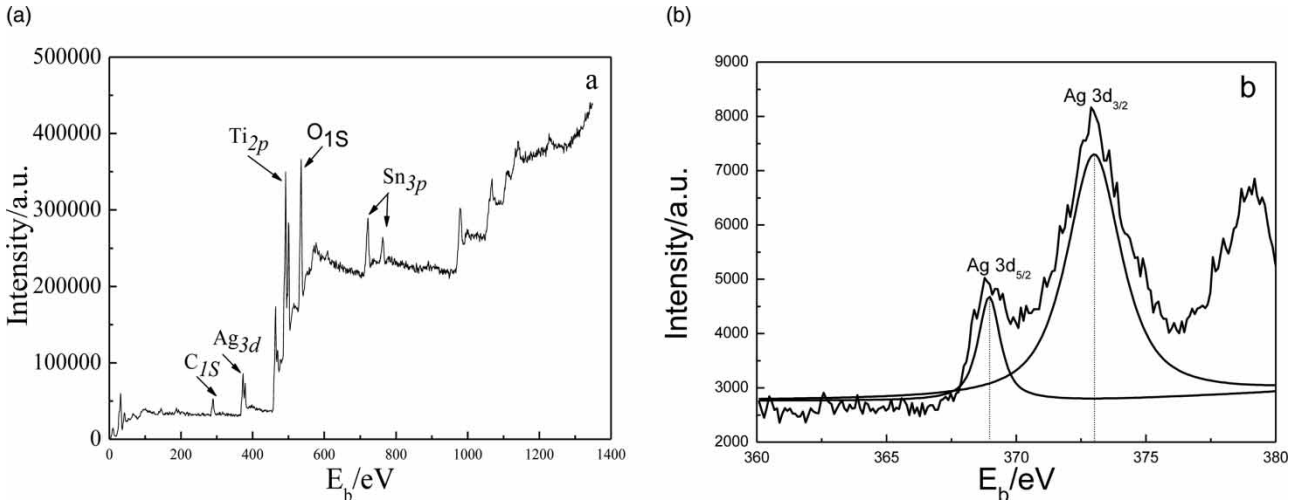

Figure 3 | The XPS spectrum of Ag/TiO_2-SnO_2 (CTAB) (a) and the XPS spectra of Ag_{3d} (b).

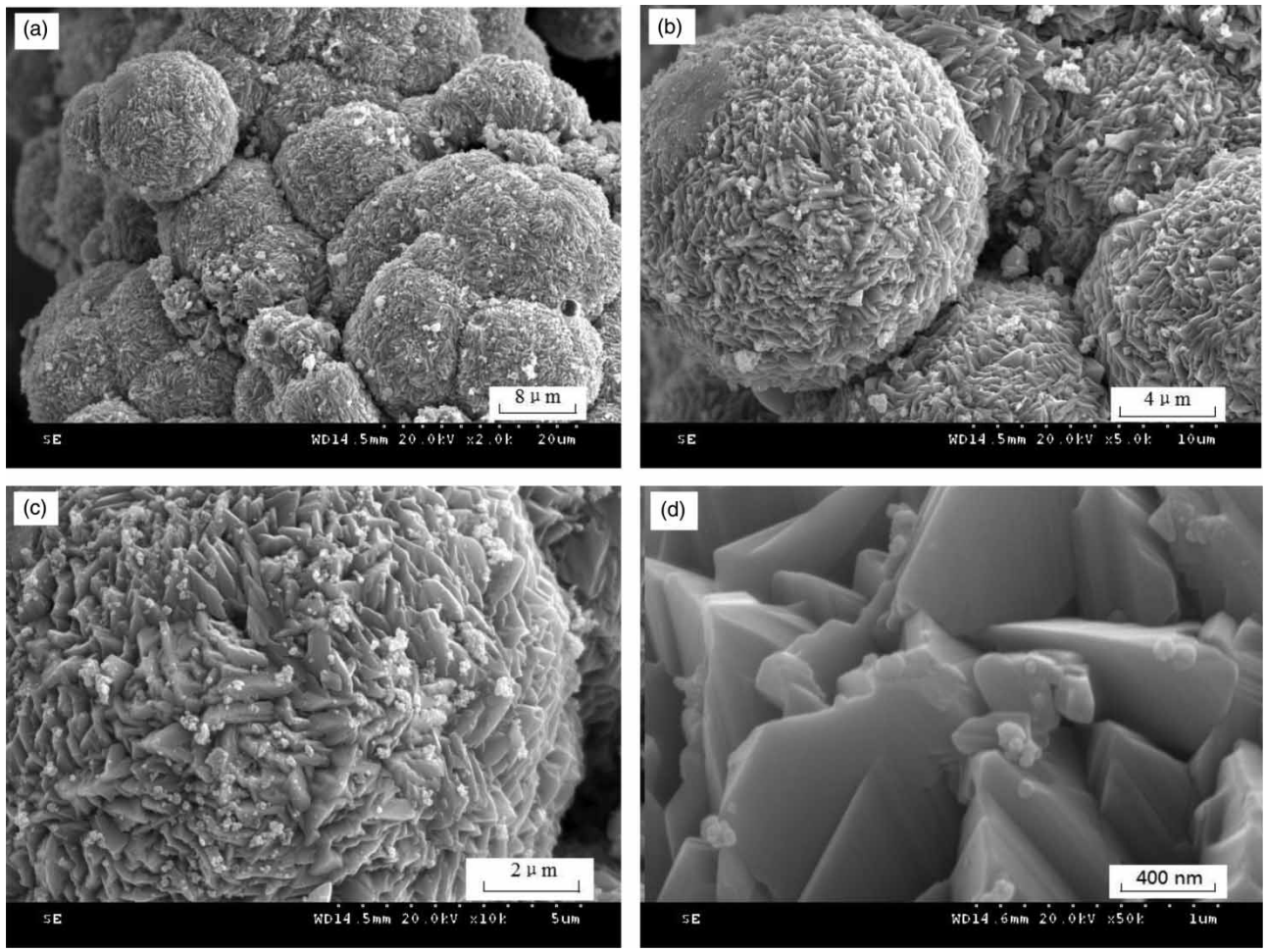

Figure 4 | SEM images of Ag/TiO_2-SnO_2 (CTAB).

the agglomeration of particles, and the morphology of the products can have a certain growth pattern (Wu *et al.* 2010). In addition, the interaction between TiO_2 and SnO_2 makes a new compound, $SnTiO_4$, which facilitates the sample particle aggregation (Kiraz *et al.* 2011). So the interaction of three factors forms the unique coral-globular structure.

As seen morphologies of Ag/TiO_2-SnO_2 (CTAB), Ag/TiO_2-SnO_2, TiO_2-SnO_2 (CTAB), and TiO_2-SnO_2, four kinds of composites were analyzed by SEM. From Figure 5(a) and 5(b), it can be seen differences of these morphologies, and the product with the template CTAB shows a regular coral-globular structure. However, the sample without CTAB template exhibits a lot of dispersed small particles and big nanosheet, due to the addition of CTAB that can change the growth direction of the composite material by the electrostatic and steric effects. At the same time, from Figure 5(a) and 5(c), we can find that Ag also has a certain effect on the growth morphology of the product during the synthesis process, because Ag can affect the internal structure of the product. By comparing the morphology of TiO_2-SnO_2 (CTAB) and TiO_2-SnO_2, Ag has played the key role in the formation of the coral-globular structure (Li *et al.* 2015). Thereby, the formation of coral-globular structure is mainly caused by the integrated effects of noble metal Ag and the action of CTAB, and coral-globular structure can increase the specific surface area of the product, even affecting its photocatalytic activity.

SEM-EDS analysis

The element content of Ag/TiO_2-SnO_2 (CTAB) composite was studied by the SEM-EDS analysis, shown in Figure 6. As seen in Figure 6, Ag/TiO_2-SnO_2 (CTAB) composite material is made up of O, Ti, Sn and Ag elements, and no other impurity elements. CTAB initiating in the early stage

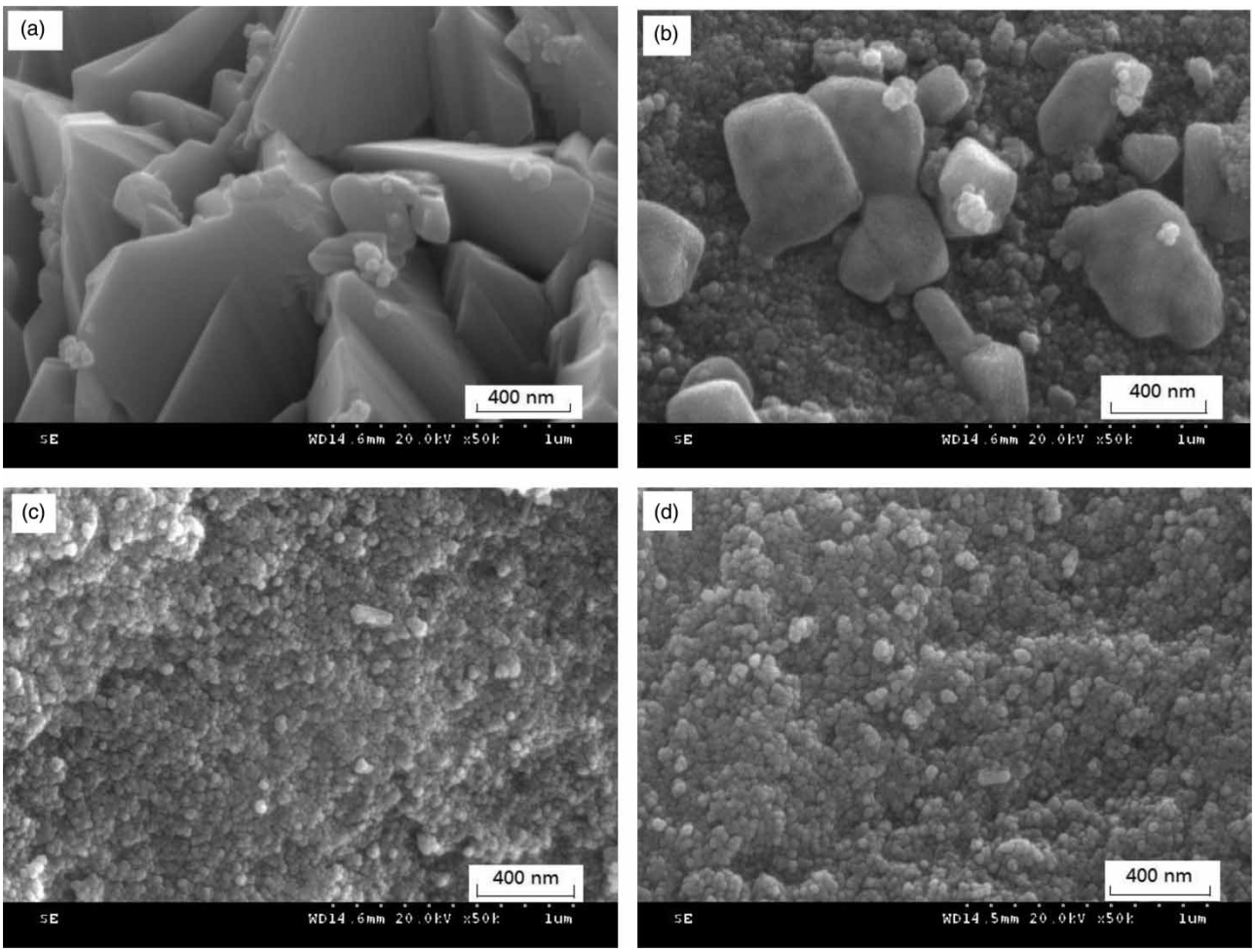

Figure 5 | SEM images of different products of Ag/TiO_2-SnO_2 (CTAB) (a), Ag/TiO_2-SnO_2 (b), TiO_2-SnO_2 (CTAB) (c), and TiO_2-SnO_2 (d).

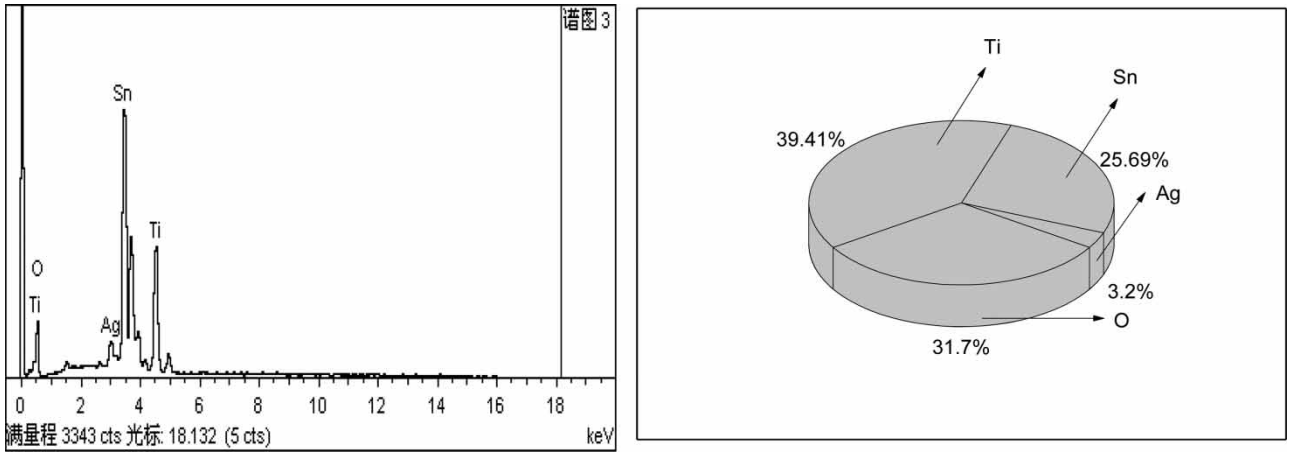

Figure 6 | The EDS spectrum of as-synthesized Ag/TiO_2-SnO_2 (CTAB) (left) and the actual element content in the as-synthesized Ag/TiO_2-SnO_2 (CTAB) (right).

has been completely removed by a calcination step, further eliminating the existence of C elements in the XPS spectra. The content of all elements of Ag/TiO_2-SnO_2 (CTAB) composite shows that the actual element content is close to the theory content of the feed ratio; there is no big loss in the synthesis process.

N_2 adsorption–desorption analysis

N_2 adsorption–desorption analysis was carried out to evaluate the surface physicochemical properties of as-synthesized materials; the results shown in Figure 7. From Figure 7, Ag/TiO_2-SnO_2 (CTAB), Ag/TiO_2-SnO_2, TiO_2-SnO_2 (CTAB),

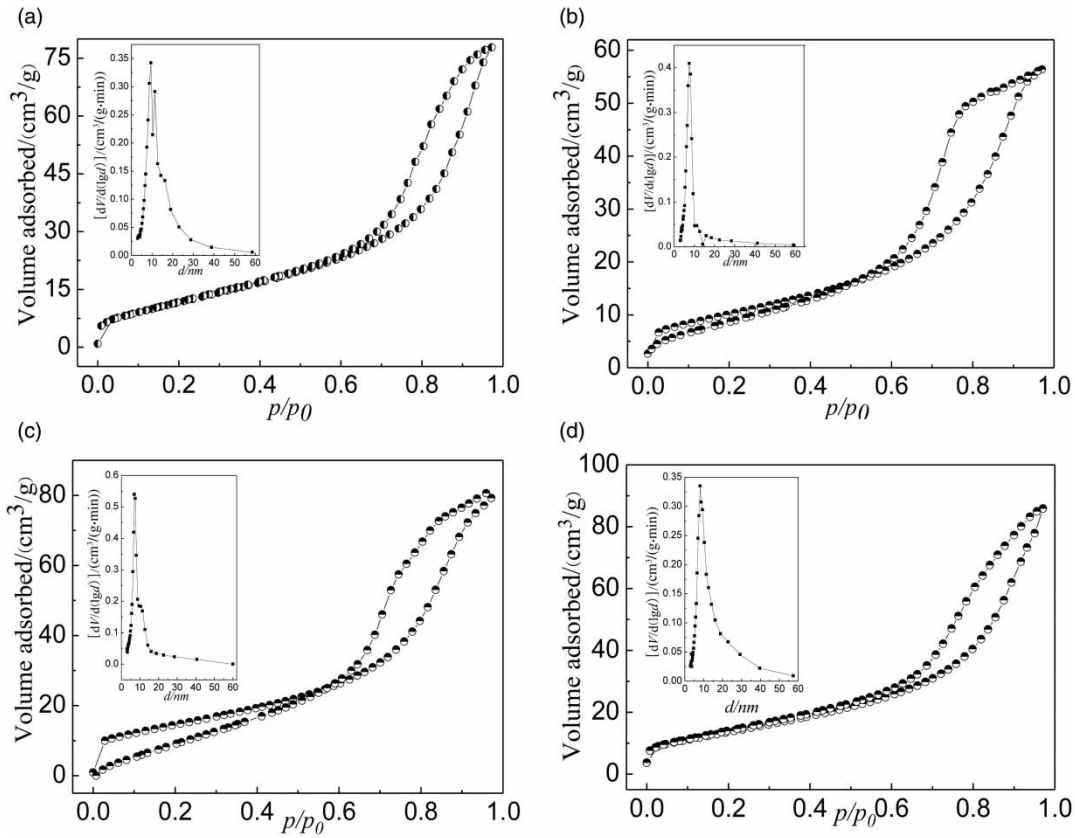

Figure 7 | N_2 adsorption–desorption isotherms and pore size distribution curves of Ag/TiO_2-SnO_2 (CTAB) (a), Ag/TiO_2-SnO_2 (b), TiO_2-SnO_2 (CTAB) (c), and TiO_2-SnO_2 (d).

and TiO_2-SnO_2 composite materials have the isotherm of type IV shape, indicating the presence of the mesoporous structure; in addition, the shape of the hysteresis loop belongs to H1 type, in which pore structure comes from the most typical cylinder hole opening at both ends.

The Brunauer–Emmett–Teller (BET) surface area (S_{BET}), average pore size and pore volume of the four kinds of composite materials are shown in Table 1. Results show that the specific surface area of the sample Ag/TiO_2-SnO_2 (CTAB) is better than that of Ag/TiO_2-SnO_2, but the BET value of the sample with doping of Ag decreases, attributed to its morphology changes. According to SEM images, the composite material formed by the Ag deposition is composed of the spherical coral and irregular quartet structure, respectively, and these particles are bigger, which can make the specific surface area of composites be smaller. In addition, pore size distribution curves of these composite materials show that the pore structure and the distribution of composite materials are more uniform. The pore size distribution curve of Ag/TiO_2-SnO_2 (CTAB) forms two relatively concentrated areas at 2 nm and 11.3 nm, mainly due to the structure of the coral globule.

Photocatalytic activity

As-synthesized samples were applied to remove RhB as the model molecule in water to investigate their photocatalytic activities under multi-mode degradation, and photocatalytic experiments were carried out; results as shown in Figure 8. From Figure 8(a), the degradation efficiency of Ag/SnO_2-TiO_2 (CTAB) is higher than those of the commercial TiO_2, Ag/TiO_2-SnO_2 (without using the template CTAB), TiO_2-SnO_2 (CTAB), and TiO_2-SnO_2 under the same condition. As shown in Figure 8(c), the photocatalytic experiment is carried out under UV light irradiation in 120 min, and the absorption peak of RhB becomes low with the time increasing until it disappears. The results of reaction kinetics of photocatalytic activity under UV light irradiation (Figure 8(b)) show that their linear simulations can be seen as a pseudo-first-order reaction kinetics. The catalyst recycling process (Figure 8(d)) shows that the photocatalytic activity of Ag/TiO_2-SnO_2 (CTAB) can be kept even after three cycles, indicating good photocatalytic capability and a certain practical value.

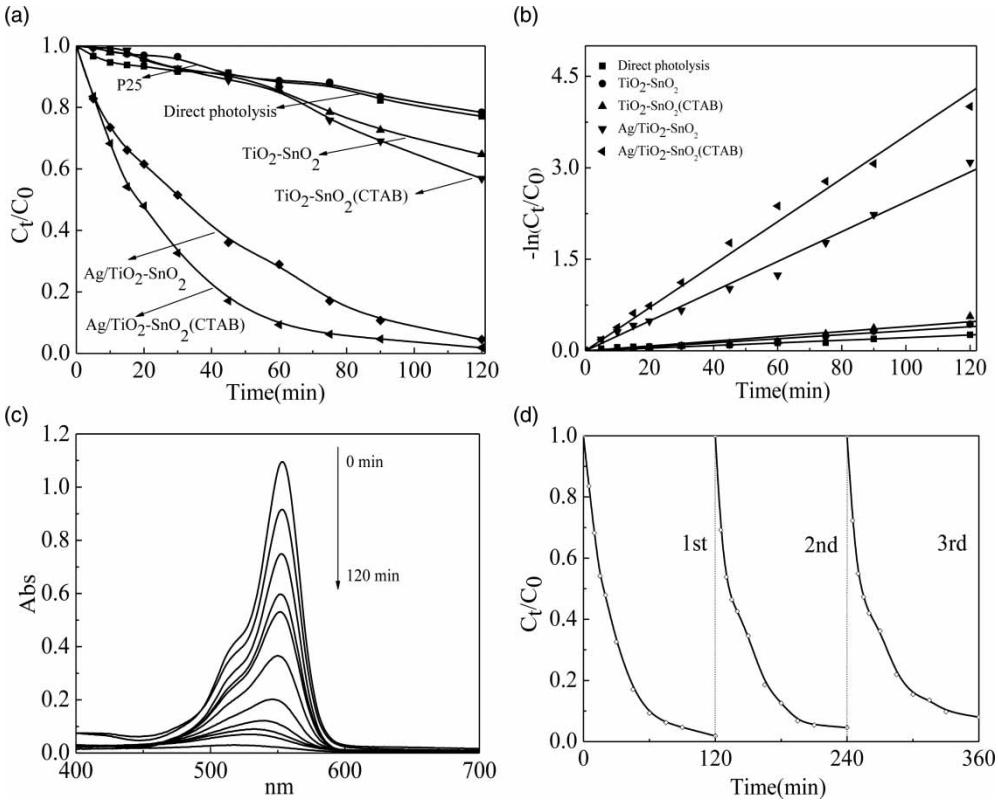

Figure 8 | UV photocatalytic degradation of RhB using different photocatalysts (a), kinetics of UV photocatalytic degradation of RhB using different photocatalysts (b), UV photocatalytic degradation of RhB using Ag/TiO_2-SnO_2 (CTAB) (c), and photocatalytic activities of Ag/TiO_2-SnO_2 (CTAB) under UV irradiation for degradation of RhB after three cycles (d).

In addition, the photocatalytic activities under multimode were used to investigate the effect of composite degradation of RhB under different light sources including ultraviolet (Figure 8(a)), simulated sunlight (Figure 9(a)), visible light (Figure 9(b)) and microwave-assisted photocatalysis (Figure 9(c)). Results show that the photocatalytic activity of Ag/SnO_2-TiO_2 (CTAB) composite is higher than those of RhB direct photocatalysis, commercial TiO_2, Ag/TiO_2-SnO_2 (without using the template CTAB), TiO_2-SnO_2 (CTAB), and TiO_2-SnO_2 under different light sources. At the same time, the photocatalytic activity of Ag/SnO_2-TiO_2 (CTAB) for degrading different organic pollutants (selecting four kinds of dyes and an organic acid) (Figure 9(d)) shows different degrees of degradation effects under UV light irradiation, indicating that its photocatalytic effect has universality.

The photocatalytic activity of Ag/TiO_2-SnO_2 (CTAB) is better than those of Ag/TiO_2-SnO_2 (without using the template CTAB), TiO_2-SnO_2 (CTAB), and TiO_2-SnO_2 under the same condition and the reasons may be as follows. (1) Noble metal Ag can effectively capture photogenerated electrons and promote the transfer of photogenerated electrons; photogenerated electrons reacting with the oxygen adsorbed on the surface of composites to form superoxide radical. (2) Ag/TiO_2-SnO_2 (CTAB) has certain visible light absorption for the SPR effect of Ag, which can improve the utilization rate of light. The addition of silver can reduce the band gap energy of composites and increase the range of light response in the visible region. According to the photocatalytic degradation activity of the four kinds of composites, it can be found that the photocatalytic activity of composites increases with the addition of silver. (3) SnO_2 is reacted with TiO_2, generating $SnTiO_4$ in the composite process, so that the photocatalytic activity of the composite is enhanced due to the existence of $SnTiO_4$. (4) The influence of Ag and CTAB on the morphology and structure of as-synthesized samples and the special morphology can increase scattering of light and effective transfer of carriers. Ag can affect the structure of the product, and CTAB can affect the growth process of the composite through the electrostatic and steric effects such that a double layer forms on the surface of particles. In addition, the product presents a coral-globule structure with the action of CTAB and Ag, and this special structure plays a key role in the photocatalytic degradation activity of Ag/TiO_2-SnO_2 (CTAB) composite material.

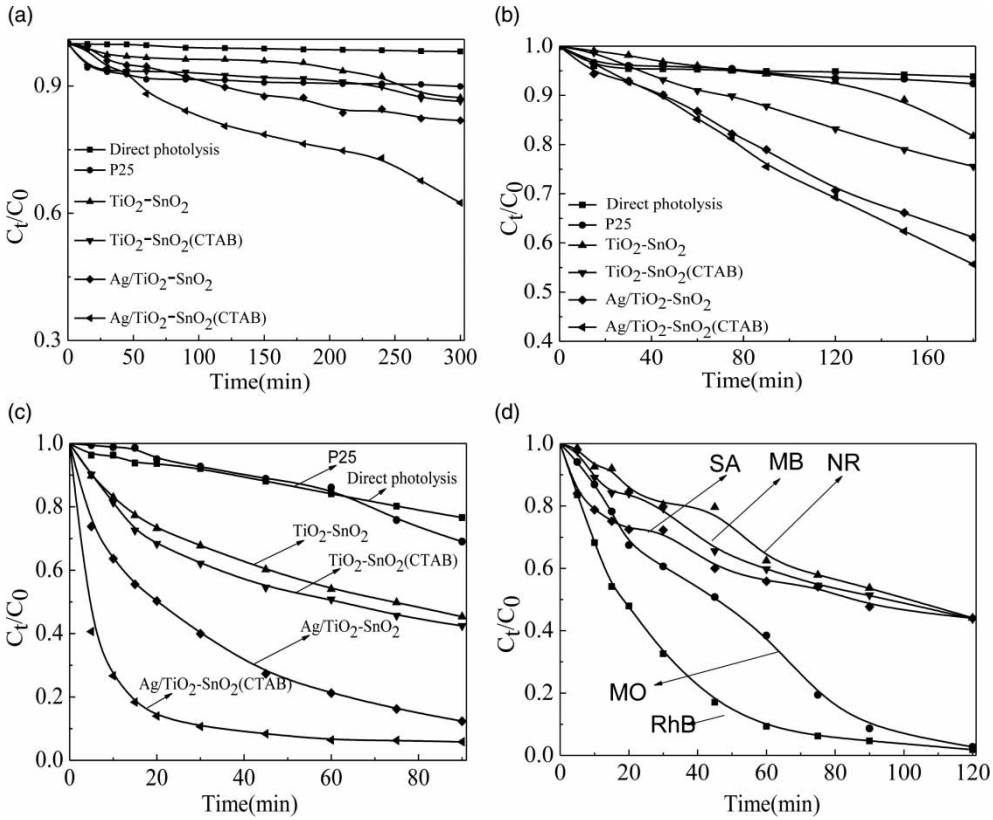

Figure 9 | Photocatalytic degradation of RhB under simulated solar light (a), visible light (b), and microwave-assisted (c). Degradation of different organic pollutants by Ag/TiO_2-SnO_2 (CTAB) under UV light (d).

In summary, the photocatalytic degradation activity of composites can be attributed to the different specific surface area, the photogenerated electrons captured by Ag, and the effective transfer of the photogenerated electron–hole pairs caused by the special structure of the composite.

Capture experiment and possible photocatalytic mechanism

Photocatalytic experiments were used to predict the possible mechanism of Ag/SnO_2-TiO_2 (CTAB) by adding capture agents including tert-butanol (TBA, capture superoxide $\cdot O_2^-$), methanol (MT, capture ·OH), and EDTA (capture h^+) during photocatalytic degradation of RhB with Ag/SnO_2-TiO_2 (CTAB) under UV irradiation, as shown in Figure 10. Compared to the photocatalytic degradation of Ag/SnO_2-TiO_2 (CTAB), the degradation efficiency decreases after adding TBA, which is the superoxide ($\cdot O_2^-$) capture agent, indicating that most of the superoxide free radicals in the photocatalytic system are captured. At the same time, the photocatalytic activity of Ag/SnO_2-TiO_2 (CTAB) also decreases to a certain degree after adding MT or EDTA. The superoxide free radical in the photocatalytic reaction system is the main active substance, and ·OH and h^+ also have a certain role. These active groups are the basis of photocatalytic degradation of pollutants, which can be used to speculate about the possible photocatalytic mechanism.

Figure 11 illustrates the photocatalytic mechanism of the photoinduced charge separation, migration and degradation process of dye molecule under UV light irradiation. Both TiO_2 and SnO_2 are wide-band-gap semiconductors, and the band gap energy of SnO_2 (3.8 eV) is higher than that of TiO_2 (3.2 eV). The Fermi level of TiO_2 is lower

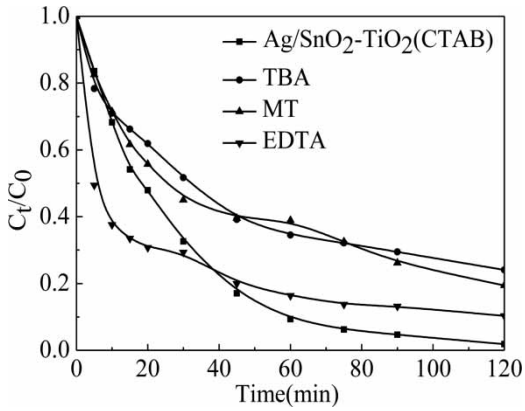

Figure 10 | Capture experiment results of Ag/TiO_2-SnO_2 (CTAB) composite.

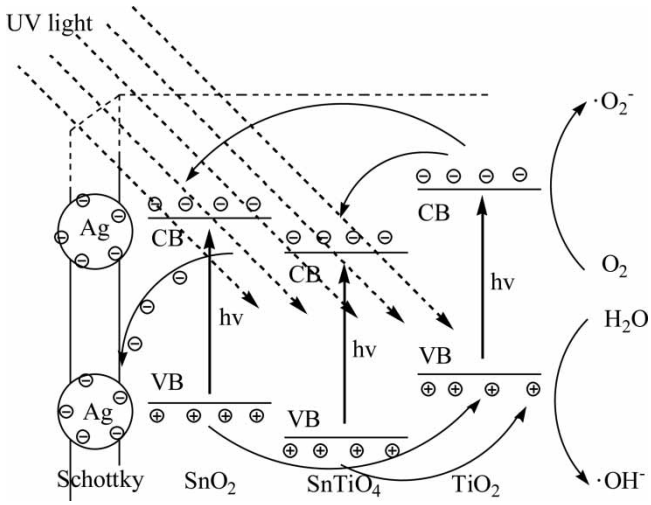

Figure 11 | Possible photocatalytic reaction mechanism of Ag/TiO_2-SnO_2 (CTAB) composite.

than that of SnO_2, meanwhile, and a new substance, $SnTiO_4$, is produced in the composite and its band gap value is low (Knauf *et al.* 2015). Therefore, considering the conduction band and the valence band of TiO_2, SnO_2, and $SnTiO_4$, on the one hand, photogenerated electrons are easy to shift from TiO_2 to SnO_2 and $SnTiO_4$. On the other hand, photogenerated holes on the interface also take part in the reaction. The $SnTiO_4$ can prolong the separation time of photogenerated electron–hole pairs to an extent. In addition, the work function (Φ_m) of Ag is much higher than that of TiO_2 and SnO_2. Therefore, the Fermi level of Ag is below the Fermi level of TiO_2 and SnO_2. Photogenerated electrons can move from the conduction band of the semiconductor to Ag, forming a space charge layer. In the charge layer, positive charge surplus is on the surface of the semiconductor, and the surface of Ag will receive the excess negative charge. The Schottky barrier formed at the metal–semiconductor interface can capture electrons in the process of photocatalysis, and prevent the electron–holes recombining and then improve the photocatalytic activity (Logar *et al.* 2010). The possible photocatalytic mechanism is shown in Figure 11.

CONCLUSION

Taking CTAB as the template, using TiO_2 as the substrate, coral-globular-like composite Ag/TiO_2-SnO_2 (CTAB) was successfully synthesized by the sol–gel combined with temperature-programmed treatment method. The composite material has a good crystalline structure, and the

morphology is uniform coral-globular. Ag/TiO_2-SnO_2 (CTAB) shows the highest photocatalytic activity under multi-mode photocatalytic experiments, due to the SPR effect of noble metal Ag, the template action of CTAB, and the specific surface area. Meanwhile, the special morphology provides a convenient way of charge carrier transfer, which can effectively promote the separation of electrons and holes. The SPR effect of Ag can form the Schottky barrier on the metal semiconductor surface to achieve the purpose of improving photocatalytic activity. Electrostatic and steric effects of CTAB can affect the crystal growth of Ag/TiO_2-SnO_2 (CTAB) to change the morphology and the specific surface area.

ACKNOWLEDGEMENTS

This study was supported by the National Natural Science Foundation of China (21376126), Natural Science Foundation of Heilongjiang Province, China (B201106), Scientific Research of Heilongjiang Province Education Department (12511592), Government of Heilongjiang Province Postdoctoral Grants, China (LBH-Z11108), Open Project of Green Chemical Technology Key Laboratory of Heilongjiang Province College, China (2013), Postdoctoral Researchers in Heilongjiang Province of China Research Initiation Grant Project (LBH-Q13172), Innovation Project of Qiqihar University Graduate Education (YJSCX2015-ZD03), College Students' Innovative Entrepreneurial Training Program Funded Projects of Qiqihar University (201610221112), and Qiqihar University in 2016 College Students Academic Innovation Team Funded Projects.

REFERENCES

Beltran, A., Andres, J. & Sambrano, J. R., 2008 Density functional theory study on the structural and electronic properties of low index rutile surfaces for TiO_2/SnO_2/TiO_2 and SnO_2/TiO_2/SnO_2 composite systems. *J. Phys. Chem. A.* **112** (38), 8943–8952. DOI: 10.1021/jp801604n.

Chen, D., Jiao, X. & Zhang, M. 2000 Hydrothermal synthesis and characterization of $(Zr_{1-x}Sn_x)TiO_4$ (x = 0.05–0.20) powders. *Mater. Res. Bull.* **35** (13), 2101–2108. DOI: 10.1016/S0025-5408(00)00418-9.

Chen, X. P., Chen, W., Lin, P. B., Yang, Y., Gao, H. Y., Yuan, J. & Shangguan, W. F. 2013 In situ photodeposition of nickel oxides on CdS for highly effectual hydrogen production via visible-light-driven photocatalysis. *Catal. Commun.* **36** (5), 104–108. DOI: 10.1016/j.catcom.2013.03.016.

Chen, Y. F., Huang, W. X., He, D. L., Situ, Y. & Huang, H. 2014 Construction of heterostructured g-C_3N_4/Ag/TiO_2 microspheres with enhanced photocatalysis performance under visible-light irradiation. *Appl. Mater. Interf.* **6**, 14405–14414. DOI: 10.1021/am503674e.

Dimitrijevic, N. M., Tepavcevic, S., Liu, Y. Z. & Rajh, T. 2013 Nanostructured TiO_2/polypyrrole for visible light photocatalysis. *J. Phys. Chem. C* **117**, 15540–15544. DOI: 10.1021/jp405562b.

Fan, Q. H., Tan, X. L., Li, J. X., Wang, X. K., Wu, W. S. & Montavon, G. 2009 Sorption of Eu(III) on attapulgite studied by batch, XPS and EXAFS techniques. *Environ. Sci. Technol.* **43** (15), 5776–5782. DOI: 10.1021/es901241f.

Gao, Y. F., Masuda, Y., Ohta, H. & Koumoto, K. 2004 Room-temperature preparation of ZrO_2 precursor thin film in an aqueous peroxozirconium-complex solution. *Chem. Mater.* **16** (13), 2615–2622. DOI: 10.1021/cm049771i.

Jiang, Y., Deng, J. G., Xie, S. H., Yang, H. G. & Dai, H. X. 2015 Au/MnO_x/3DOM $La_{0.6}Sr_{0.4}MnO_3$: highly active nanocatalysts for the complete oxidation of toluene. *Ind. Eng. Chem. Res.* **54** (3), 900–910. DOI: 10.1021/ie504304u.

Katoch, A., Kim, J. H., Kwon, Y. J., Kim, H. W. & Kim, S. S. 2015 Bifunctional sensing mechanism of SnO_2–ZnO composite nanofibers for drastically enhancing the sensing behavior in H_2 gas. *Appl. Mater. Interfaces* **7** (21), 11351–11358. DOI: 10.1021/acsami.5b01817.

Kiraz, N., Burunkaya, E. & Kesmez, O. 2011 Preparation of Sn doped nanometric TiO_2 powders by reflux and hydrothermal syntheses and their characterization. *J. Sol-Gel Sci. Technol.* **59** (2), 381–386. DOI: 10.1007/s10971-011-2515-7.

Knauf, R. R., Kalanyan, B., Parsons, G. N. & Dempsey, J. L. 2015 Charge recombination dynamics in sensitized SnO_2/TiO_2 core/shell photoanodes. *J. Phys. Chem. C* **119** (51), 28353–28360. DOI: 10.1021/acs.jpcc.5b10574.

Kobayashi, R., Tanigawa, S., Takashima, T., Ohtani, B. & Irie, H. 2014 Silver-inserted heterojunction photocatalysts for Z-Scheme overall pure-water splitting under visible-light irradiation. *J. Phys. Chem. C* **118** (39), 22450–22456. DOI: 10.1021/jp5069973.

Kumar, M. & Deka, S. 2014 Multiply twinned AgNi alloy nanoparticles as highly active catalyst for multiple reduction and degradation reactions. *Appl. Mater. Interfaces* **5** (13), 16071–16081. DOI: 10.1021/am503913y.

Li, G. Q., Wang, D. F., Zou, Z. G. & Ye, J. H. 2008 Enhancement of visible-light photocatalytic activity of $Ag_{0.7}Na_{0.3}NbO_3$ modified by a platinum complex. *J. Phys. Chem. C* **112**, 20329–20333. DOI: 10.1021/jp803864j@proofing.

Li, M. H., Maria Eugenia, N. T., Nereyda, N. M., Catalina, M. J., Wang, J. W., Robert, D., Facundo, R. & Hoek, E. M. V. 2011 Synergistic bactericidal activity of Ag-TiO_2 nanoparticles in both light and dark conditions. *Environ. Sci. Technol.* **45**, 8989–8995. DOI: 10.1021/es201675m.

Li, T. Y., Liu, Y. H., Chitara, B. & Goldberger, J. E. 2014a Li inercalation into 1D TiS_2 (en) chains. *J. Am. Chem. Soc.* **136** (8), 2986–2989. DOI: 10.1021/ja4132399.

Li, L., Zhang, X. L., Zhang, W. Z., Wang, L. L., Chen, X. & Gao, Y. 2014b Microwave-assisted synthesis of nanocomposite

Ag/ZnO–TiO_2 and photocatalytic degradation rhodamine B with different modes. *Colloids and Surfaces A* **457**, 134–141. DOI: 10.1016/j.colsurfa.2014.05.060.

Li, L., Wang, L. L., Zhang, W. Z., Zhang, X. L., Chen, X. & Dong, X. 2014c Urchin-like CdS/ZrO_2 nanocomposite prepared by microwave-assisted hydrothermal combined with ion-exchange and its multimode photocatalytic activity. *J. Nanopart. Res.* **16**, 2753. DOI: 10.1007/s11051-014-2753-z.

Li, L., Huang, X. D., Zhang, J. Q., Zhang, W. Z., Ma, F. Y., Xiao, Z. X., Gai, S., Wang, D. D. & Li, N. 2015 Multi-layer three-dimensionally ordered bismuth trioxide/titanium dioxide nanocomposite: synthesis and enhanced photocatalytic activity. *J. Colloid. Interf. Sci.* **443**, 13–22. DOI:10.1016/j.jcis.2014.11.062.

Liang, J. F., Zhao, Y., Guo, L. & Li, L. D. 2012 Flexible free-standing graphene/SnO_2 nanocomposites paper for Li-ion battery. *ACS Appl. Mater. Interf.* **4** (11), 5742–5748. DOI: 10.1021/am301962d.

Liao, S. J., Chen, T., Miao, C. X., Yang, W. M., Xie, Z. K. & Chen, Q. L. 2008 Effect of TiO_2 on the structure and catalytic behavior of iron–potassium oxide catalyst for dehydrogenation of ethylbenzene to styrene. *Catal. Commun.* **9** (9), 1817–1821. DOI: 10.1016/j.catcom.2008.02.009.

Logar, M., Jancar, B., Sturm, S. & Suvorov, D. 2010 Weak polyion multilayer-assisted in situ synthesis as a route toward a plasmonic Ag/TiO_2 photocatalyst. *Langmuir* **26** (14), 12215–12224. DOI: 10.1021/la101124q.

Merrill, N. A., Sethi, M. & Knecht, M. R. 2013 Structural and equilibrium effects of the surface passivant on the stability of Au nanorods. *ACS Appl. Mater. Interf.* **5** (16), 7906–7914. DOI: 10.1021/am401997q.

Mishra, S., Jeanneau, E., Berger, M. H., Hochepied, J. F. & Daniele, S. 2010 Novel heteroleptic heterobimetallic alkoxide complexes as facile single-source precursors for Ta^{5+} doped TiO_2-SnO_2 nanoparticles. *J. Inorg. Chem.* **49** (23), 11184–11189. DOI: 10.1021/ic102134w.

Pan, J., Song, X. F., Zhang, J., Shen, H. & Xiong, Q. H. 2011 Switchable wettability in SnO_2 nanowires and SnO_2@ SnO_2 heterostructures. *J. Phys. Chem. C* **115** (45), 22225–22231. DOI: 10.1021/jp207376t.

Shan, H., Liu, C. B., Liu, L., Zhang, J. B., Li, H. Y., Liu, Z. & Zhang, X. B. 2013 Excellent toluene sensing properties of SnO_2–Fe_2O_3 interconnected nanotubes. *ACS Appl. Mater. Interf.* **5** (13), 6376–6380. DOI: 10.1021/am4015082.

Wu, T. S., Wang, K. X., Li, G. D., Sun, S. Y., Sun, J. & Chen, J. S. 2010 Montmorillonite-supported Ag/TiO_2 nanoparticles: an efficient visible-light bacteria photodegradation material. *ACS Appl. Mater. Interf.* **2** (2), 544–550. DOI: 10.1021/am900743d.

Xu, L., Steinmiller, E. M. P. & Skrabalak, S. E. 2012 Achieving synergy with a potential photocatalytic Z-Scheme: synthesis and evaluation of nitrogen-doped TiO_2-SnO_2 composites. *J. Phys. Chem. C* **116** (1), 871–877. DOI: 10.1021/jp208981 h.

Yuan, S. M., Li, J. X., Yang, L. T., Su, L. W., Liu, L. & Zhou, Z. 2011 Preparation and lithium storage performances of mesoporous Fe_3O_4@C microcapsules. *ACS Appl. Mater. Interf.* **3** (3), 705–709. DOI: 10.1021/am1010095.

First received 22 February 2017; accepted in revised form 15 May 2017. Available online 29 June 2017